CAL-X: AN X-RAY RADIOGRAPHY TOOL FOR HIGH THROUGHPUT COREFLOOD EXPERIMENTATION. APPLICATIONS IN THE EOR CONTEXT.

Souhail Youssef, Matthieu Mascle, Yannick Peysson, Olga Vizika

IFP Energies nouvelles, 1&4 avenue de Bois-Préau, Rueil-Malmaison, France

This paper was prepared for presentation at the International Symposium of the Society of Core Analysts held in Vienna, Austria 28 August - 1 September 2017

ABSTRACT

To speed up coreflood experiments, we have developed a state of the art experimental setup (CAL-X) designed for high throughput coreflood experimentation. The setup is composed of an X-ray radiography facility, a fully instrumented multi-fluid injection platform and a dedicated X-ray transparent core holder. The equipment was designed to handle small samples of 10 mm in diameter and 20 mm in length, and can be operated at up to 150 bar and 150 °C. The X-ray facility consists of a high-power X-ray tube and a high speed-low noise detector allowing real-time radiography acquisition and offering sufficient density resolution to use dopant-free fluids. The injection platform is fully automated and allows the control and monitoring of different parameters (pressure, temperature, flow rate…). 1-D and 2-D saturation profiles are followed in real-time, allowing a precise determination of the recovery curve, reducing thus drastically time-consuming effluent measurements. Using this setup, a typical coreflood experiment can be run in less than a day. To validate the setup, we have run a series of experiments on water-wet sandstone samples to determine capillary desaturation curve, steady-state relative permeabilities and recovery factor for a formulation designed for high temperature conditions (110°C). The results show good repeatability as well as good agreement when compared to standard coreflood experiments. In the recovery factor experiment, during surfactant injection, the formation and displacement of an oil bank was observed, yielding a recovery factor of 92% OOIP.

INTRODUCTION

Demonstrating the viability of a chemical EOR project requires a meticulous and intensive laboratory study that involves complex, time-consuming workflows and optimization processes. These workflows include successive or iterative steps starting from reservoir fluid and rock characterizations followed by surfactant formulation screening and optimization, coreflood validation and simulation, and sensitivity studies [1]. In this context, High Throughput Experimentations (HTE) are necessary to decrease time and cost of laboratory studies [2]. On the chemical

side, formulation design is already performed via an efficient High Throughput Screening (HTS) methodology using a robotic platform. On the petrophysical side, fast coreflood experiments are also needed to measure EOR related petrophysical properties on different rock-facies and evaluate the efficiency of the selected formulations at reservoir conditions.

To develop HTE, three main concepts are used: automation, parallelization and sample size reduction [3]. In the field of core analysis, automation has been developed since the 80's to accelerate workflow [4,5]. A work recently reported [6] describes a fully automated coreflood laboratory based on standard core plugs sizes. With regards to size reduction, miniaturization of coreflood experiments have been also developed recently [7–9]. In these works, the objective was to image pore scale mechanisms and local fluid saturation and not experimental time reduction. Yet, it has allowed to overcome some technical challenges related to core holder miniaturization and physical properties measurement. In the present work, we combined automation and miniaturization to accelerate SCAL measurements. To that purpose we developed a dedicated setup (CAL-X) that allows to measure different properties needed in an EOR workflow like capillary desaturation curve (CDC), relative permeability and recovery factor while reducing by an order of magnitude the time needed to run these experiments.

MATERIAL AND METHODS

Experimental setup

The setup is composed of an X-ray radiography facility, a fully instrumented multi-fluid injection platform and a dedicated X-ray transparent core holder. The X-ray facility consists of a high-power X-ray tube (up to 150 kV and 500 µA) and a high speed-low noise detector allowing real-time radiography acquisition (up to 30 fps) and offering sufficient density resolution to use dopant-free fluids. The different components are embedded in a large X-ray protection cabinet (see Figure 1.a). The core holder was adapted to small samples (mini-plug) of 10 mm in diameter and 20 mm in length, and can be operated at up to 150 bar and 150 °C. The core holder body was made of beryllium to guarantee maximum X-ray transparency and temperature resistance. Each side of the core holder is equipped with three ports (inlet, outlet and pressure tap) as well as a temperature transducer. Figure 1.c shows a possible connection configuration. The injection platform (see Figure 1.b) is equipped with eight pumps and is fully automated allowing the control and monitoring of different parameters (absolute and differential pressure, temperature, flow rate…).

X-ray Radiograph Processing

The radiographs were captured using an energy of 60 kV and current of 300 µA. The use of low voltage allows for a higher contrast between components. The spatial resolution was set to 30 µm. Radiographs were captured each second. Due

to the difference in the X-ray attenuation coefficient of the injected fluid, the X-ray radiograph shows a variation in the gray-scale intensity throughout the sample. This variation can be used to estimate the fluid saturation in specific parts of the rock. The X-ray radiographs at each second are displayed and stored on the monitoring workstation as digital images of 16-bit precision. An image consists of 1800 rows and 1450 columns of pixels. Figure 2 shows a radiograph which emphasizes the sample shape and the basic components of the core holder.

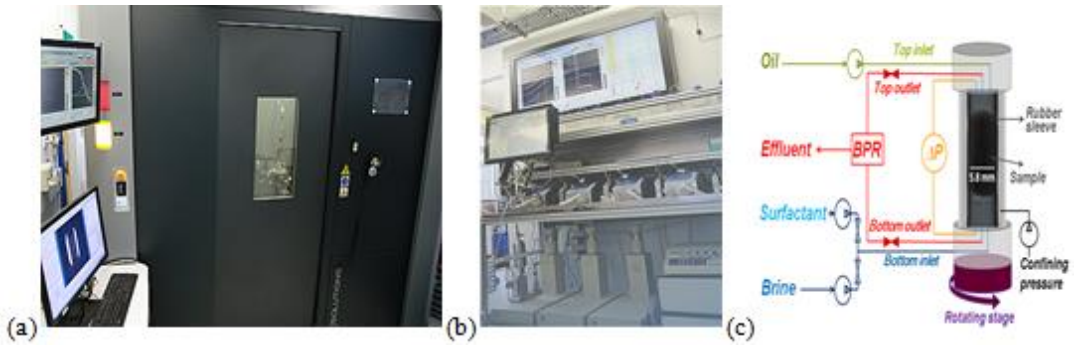

Figure 1 CAL-X setup composed of an X-ray radiography facility (a), a fully instrumented multi-fluid injection platform (b) and a dedicated X-ray transparent core holder (c).

To infer the oil saturation from the radiographs, we use Beer-Lambert's law for multi-material:

$$I = I_o \, e^{\sum_i (-\mu_i X_i)} \qquad \text{Eq.1}$$

where I and I_0 are respectively transmitted and emitted X-ray intensities, μ_i is the X-ray absorbance of the phase i, and X_i is the length of phase i.

Considering two reference states (100% water saturation and 100% oil saturation), we define I_{water} and I_{oil} as transmitted X-ray intensities:

$$I_{water} = I_o \, e^{-\mu_w X + \alpha} \qquad \text{Eq.2}$$

$$I_{oil} = I_o \, e^{-\mu_o X + \alpha} \qquad \text{Eq.3}$$

where μ_w and μ_o are the water and the oil attenuation coefficients, X is the length of the X-ray path in the fluid volume and α is a constant corresponding to the attenuation due to the solid part of the rock and the different components of the cell crossed by the X-ray. If the sample is saturated with oil and water, the transmitted X-ray intensity I_t is governed by the following equation:

$$I_t = I_o \, e^{-(\mu_o X_o + \mu_w X_w) + \alpha} \qquad \text{Eq.4}$$

where X_o and X_w are respectively the oil and the water portions in the path of the X-ray. Furthermore, by definition, we obtain the following equation:

$$X_o + X_w = X \qquad \text{Eq.5}$$

The oil saturation S_o can be obtained as follows:

$$\frac{\ln\left(\frac{I_{water}}{I_0}\right) - \ln\left(\frac{I_t}{I_0}\right)}{\ln\left(\frac{I_{water}}{I_0}\right) - \ln\left(\frac{I_{oil}}{I_0}\right)} = \frac{-\mu_w X + \mu_o X_o + \mu_w X_w}{-\mu_w X + \mu_o X} = \frac{X_o}{X} = S_o \qquad \text{Eq.6}$$

The transmitted X-ray intensity is measured by each pixel of the X-ray detector and represented by a proportional gray value. Therefore, Eq.6 can be applied directly to the gray level images to estimate local and average saturations. The results of the image processing are presented as illustrated in Figure 2.b. The upper left quadrants represent the 2D saturation map. The upper right quadrant represents the saturation profile along the sample and the lower quadrant corresponds to the evolution of mean saturation as a function of time. The radiographs are processed instantaneously allowing a real-time monitoring of experiments.

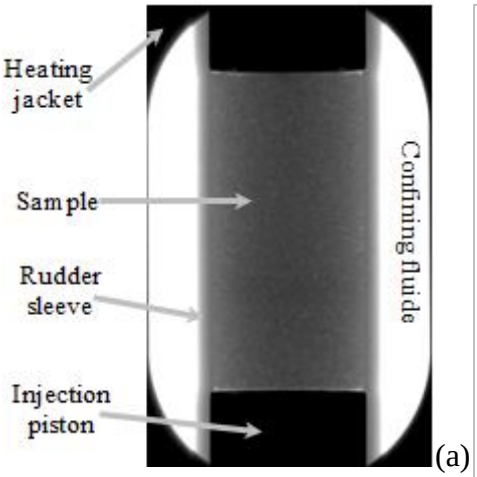

(a)

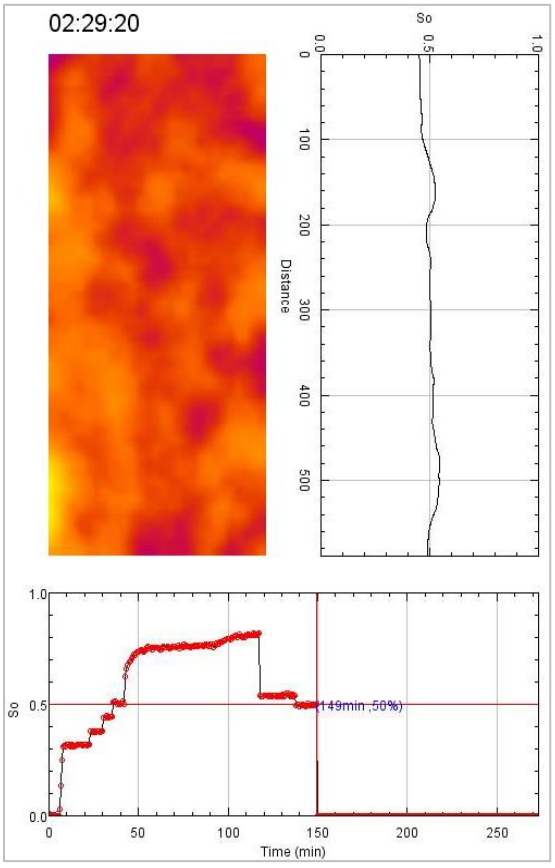

(b)

Figure 2: (a) Raw radiograph showing the sample shape and the basic components of the core holder. Illustration (b) shows an example of real-time saturation monitoring where the upper left quadrant represent the 2D saturation map. The upper right quadrant represents the saturation profile along the sample and the lower quadrant corresponds to the evolution of mean saturation as a function of time.

Rock samples

Samples used in this work are water wet outcrop sandstones from different quarries with porosity ranging from 12% to 23% and permeability ranging from 200 mD to 2030 mD (see Table 1). Samples are cored with a diamond core drill with 1 cm internal diameter and cut to a length of 2 cm. Then, they are dried in an oven for at least 48 hours at a temperature of 60 °C.

Table 1 Petrophysical properties of the plugs used in this work

Plug name	**Benth_28**	**Benth_12**	**Clash_22**	**GDF_15**
Origin	Bentheimer		Clashach	Fontainebleau
Porosity (%)	23%	22%	14%	12%
Permeability (mD)	2030	1350	950	200

APPLICATIONS AND RESULTS

Steady state relative permeability

Relative permeabilities are fundamental properties required to describe an immiscible two-phase flow using Darcy's equations. Relative permeabilities are functions of the saturation and the capillary number at which the immiscible displacement occurs. When neglecting gravity effect, Darcy's equation can be written as:

$$q_i = \frac{K_a k_{ri}(S_i, N_c) S}{\mu_i} * \frac{\Delta P_i}{L} \qquad \text{Eq.7}$$

where q_i is the volumetric flow rate of the phase i (m^3/s), K_a is the absolute permeability (m^2), k_{ri} is the relative permeability of the phase i, μ_i is the fluid viscosity (Pa.s), S_i the saturation of the phase $i, \Delta P_i$ the differential pressure measure in the phase i, between the outlet and the inlet of the plug (Pa), L the length of the plug (m) and S the cross section (m^2).

In the case of two phase flow, Steady State Method (SSM) can be used to derive relative permeability. The SSM method involves the injection of both fluids at the inlet of the plug while measuring the differential pressure and the saturation within the core. Eq.7 can then be solved analytically if capillary pressure is neglected. This condition can be assessed when fluids are injected at high flow rate. Yet, negligible capillary effect and laminar flow (i.e Reynolds number less than 10) have to be confirmed. Laminar condition is verified since a linear relation between flow rate and pressure drop is respected in mono-phasic injection. To neglected capillary pressure (Pc=0) we verify that the saturation at steady state condition is

uniform along the sample (see example on Figure 2 (b)). In this case relative permeability can be derived from Eq.7 for each fluid as:

$$\begin{cases} k_{rw}(S_w, N_c) = \dfrac{\mu_w L}{K_a S} * \dfrac{q_w}{\Delta P_w} \\ k_{rnw}(S_w, N_c) = \dfrac{\mu_{nw} L}{K_a S} * \dfrac{q_{nw}}{\Delta P_w} \end{cases} \quad \text{Eq.8}$$

where indices w and nw refer respectively to wetting and non-wetting fluids. If capillary end effects is observed, simulations must be used to derive the relative permeabilities by data history matching.

The Steady State method is usually considered as one of the most reliable methods to perform relative permeability measurements, but one of its limitations is the time required to conduct such an experiment, ranging from several days to several weeks for classical core-plug sizes. With CAL-X, the size of plugs has been decreased to reduce experimental time by an order of magnitude (i.e. few hours to few days). An example of SSM imbibition relative permeability measurement protocol is presented in Figure 3. The experiment is conducted on a water-wet Bentheimer sandstone at ambient temperature, using 25 bars of confinement pressure and 15 bars of pore pressure. For this experiment we used a 33 g/l NaCl brine and dodecane synthetic oil with respectively a viscosity of 1.07 cP and 1.52 cP. In this example, the sample is first saturated with brine for absolute permeability measurement. Then, the oil is injected at a rate of 1cc/min until steady saturation reached. Next, oil and brine are co-injected at a total flow rate of 1cc/min corresponding to a capillary number of 5 10^{-6}. The saturation S_w was computed from the X-ray imaging, the differential pressure (ΔP_w) was measured and the fluid flow rates were imposed. The relative permeabilities were measured for different saturations, S_w, by varying the fractional flow (f_i) of each phase while maintaining the total flow rate constant and then resolving Eq.8.

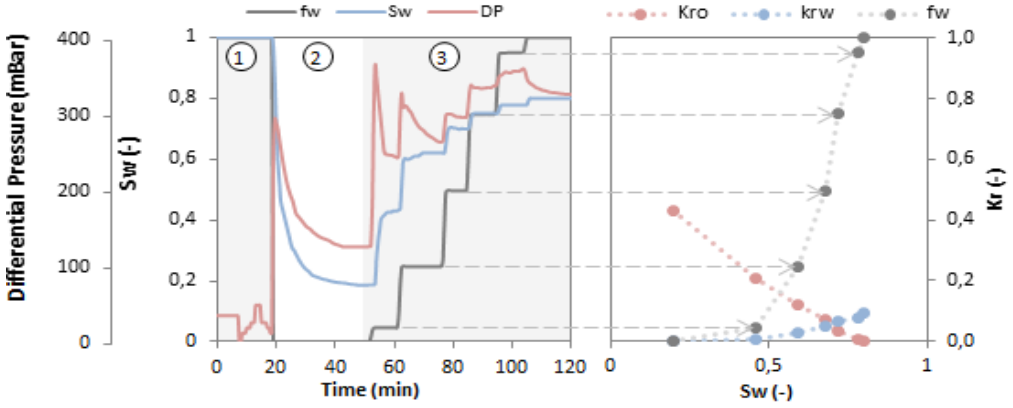

Figure 3 : Example of differential pressure ($\boldsymbol{\Delta P}$), water saturation ($\boldsymbol{S_w}$) and water fractional flow ($\boldsymbol{f_w}$) acquisition for kr measurement using SSM. The 3 steps mentioned on the 1st plot refer to the

experimental protocol. During step 3, $\boldsymbol{k_{or}(S_w)}, \boldsymbol{k_{rw}(S_w)}$ are measured for each $\boldsymbol{f_w}$ value, when the system reaches the steady state. The acquisition was conducted on a water-wet Bentheimer sandstone, with $\boldsymbol{q_{tot}^{inj} = 1\ cc/min}$ during step 3.

Left graph of Figure 3 illustrates the parameters measured during the experiment. It shows that the total time needed to run the full injection sequence is few hours. For each fractional flow, steady state is reached in about tens of minutes.

Relative permeabilities illustrated on the right graph of Figure 3 have a typical shape of Relative permeabilities measured on water-wet homogeneous sandstone. To validate the representativeness of the measurements, results are compared to macro-scale experiment. Figure 4 shows a superimposition of relative permeabilities for Benth_12 measured in this work and for a 40 mm in diameter Bentheimer plug documented in [12]. Results show a very good agreement. They demonstrate that for this homogeneous case a mini-plug can be considered to be above the representative elementary volume (REV) for multiphase flow behaviour.

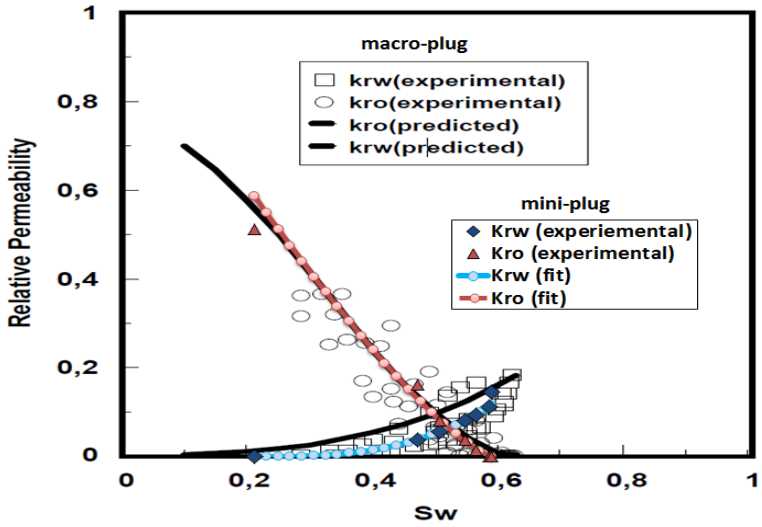

Figure 4: Relative permeability measurements conducted on the mini-plug Benth_12 compared to the ones conducted on a standard macro-plug extracted from the work of Oren et al [12].

Capillary Desaturation Curves (CDC)

The Capillary Desaturation Curve expresses the saturation of the trapped oil in a porous medium (usually expressed as the reduction of the remaining oil in place $S_{or}(N_c)/S_{orw}$) with the increase of the capillary number Nc [10]. Capillary number value is adjusted varying the injection flow rate or fluid/fluid interfacial tension. For example, by adding surfactants in the brine the interfacial tension is decreased leading to an increase of the capillary number.

In a typical CDC measurement workflow, the plug is initially fully saturated with brine. The absolute permeability can be measured at this step. Then the plug is set

to residual water saturation (Swr) by injecting oil (dodecane) from the top of the plug to reduce the impact of gravity on the fluid displacements. Brine is first brought in contact with the plug by leaching the bottom face to perform a spontaneous imbibition and then injected at 0.05 cc/min, to set the plug to residual oil saturation (Sorw). Finally, surfactant solution is injected at increasing flow rates, from 0.005 cc/min to 1 cc/min. The reduction of the interfacial tension and the increase of the injection flow rate contribute to progressively produce the trapped oil. At each step, the corresponding capillary number and the average saturation are calculated. An illustration of saturation monitored during a CDC measurement is given in Figure 5. The CDC is measured using the saturation computed from radiographs. The saturation profile So(z) can be used to correct the measured average saturation from capillary end effects. The time needed to measure a CDC is in the range of hundreds of minutes (see Figure 5). The protocol described above to perform CDC measurements has been applied on various homogenous water-wet rock types previously presented in Table 1.

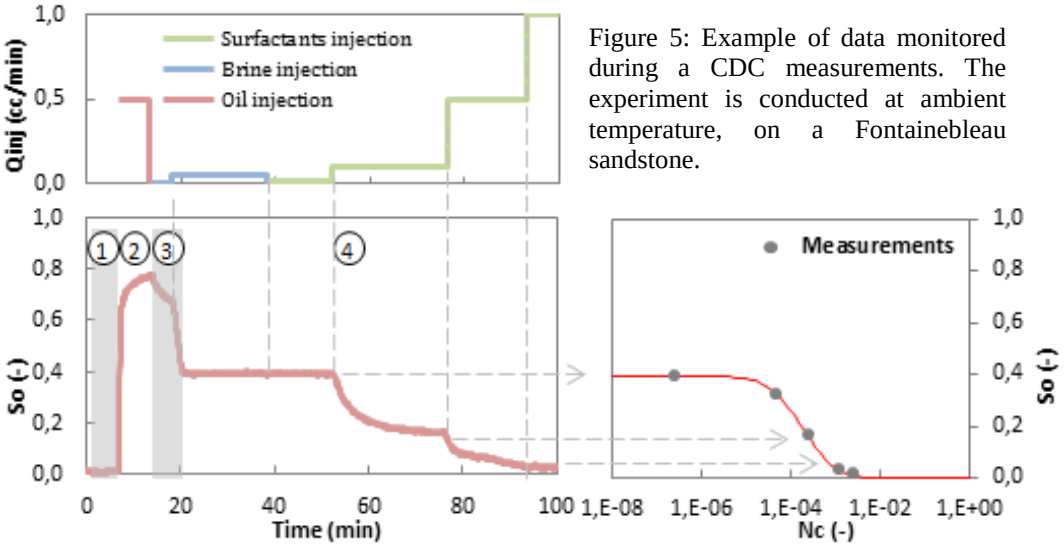

Figure 5: Example of data monitored during a CDC measurements. The experiment is conducted at ambient temperature, on a Fontainebleau sandstone.

The interfacial tensions between the surfactant solutions and oil for each test are listed in Table 2. The experimental CDC presented below are fitted using an analytical solution expressed as follows [11]:

$$\frac{S_{or}(N_c)}{S_{orw}} = \frac{1}{2}\mathrm{erfc}\left[a.\ln\left(\frac{N_c}{N_{c0}}\right)\right] \qquad \text{Eq.9}$$

where $\mathrm{erfc}(x)$ is the complementary error function, a and N_{c0} are two fitting parameters. The four measured CDC for the different mini-plugs are given in Figure 6 with the analytical fit (solid redline). Results show that all CDC have comparable tendencies with the residual oil starting to be produced for capillary

numbers higher than 10^{-5}, and half of the residual oil produced close to $N_c = 1.3\ 10^{-4}$.

Reproducible measurements have also been conducted to assess the robustness of the protocol on sample (Benth_12). The results, given in Figure 7 show very good reproducibility of the experimental CDC. To validate the representativeness of the measurements, results are compared to macro-scale experiment. The aim is to demonstrate that neither the reduced size of the mini-plugs used with CAL-X nor the measurement protocol impact the quality of the measurements. A CDC was measured on a 33 mm diameter Bentheimer sample (BH1), more detail on the experiment can be found in [13]. The results show a very good agreement between the CDC measured on mini- and macro-plug (see Figure 7).

Table 2 : The interfacial tension (IFT) is measured between the wetting phase (surfactants formulation) and the non-wetting phase (dodecane). Residual Oil Saturation reached with the brine water flush (Sorw) for the different CDC measurements. The two parameters (Nc0 and a) correspond to the fitting parameters of the analytical CDC expression.

	Benth_28	**Benth_12**	**Clash_22**	**GDF_15**
IFT (mN/m)	0.45	0.10	0.10	0.50
Sorw	0.36	0.4	0.4	0.4
Nc0	$1.\ 10^{-4}$	$1.8\ 10^{-4}$	$2.\ 10^{-4}$	$1.3\ 10^{-4}$
a	0.8	0.5	0.5	0.7

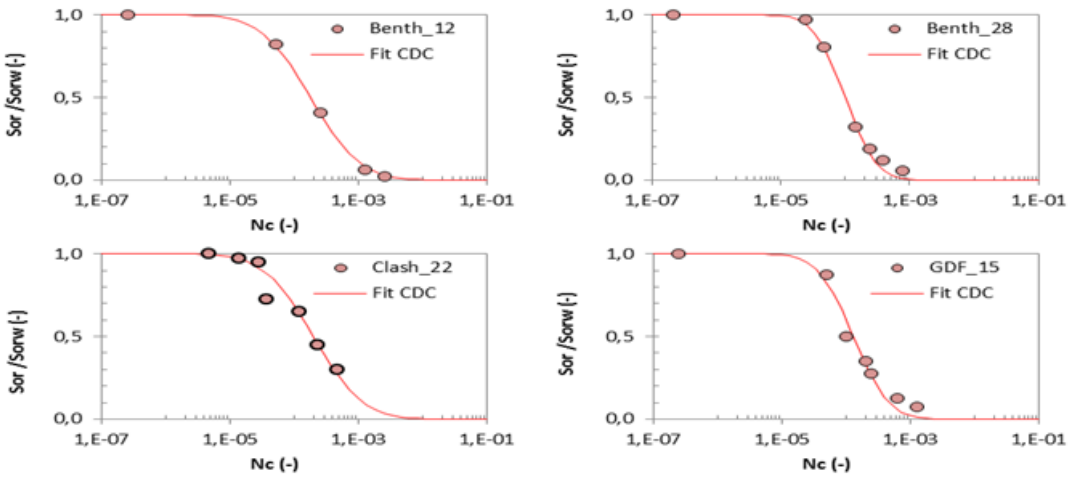

Figure 6 : Experimental CDC measured on four rock-types. The residual oil saturation Sorw reached before injecting the surfactants are given in Table 2. The four experimental curves are fitted using Eq 9, the fitting parameters are given in Table 2.

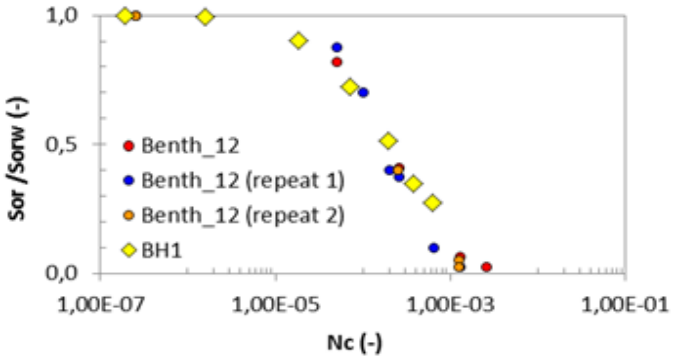

Figure 7 : CDC reproducibility measurements conducted on the mini-plug Benth_12 (circle) compared to a CDC measured on a macro-plug (BH1).

Production curves and Recovery factor (RF)

Production curves help assess the oil recovery kinetics and recovery factor when using enhanced oil recovery techniques, by reproducing the injection sequences of fluids planned in the EOR process. Recovery factor, which evaluates the recoverable part of the original oil in place (OOIP), constitutes a convenient way to compare the efficiency of different injection sequences and chemical products.

In this section, we present the use of the new equipment (CAL-X) to study infinite surfactant slug injection tests at high temperatures. The objective was to check the efficiency of a formulation designed to minimise the interfacial tension between the oil phase (dodecane) and the water phase (a 33 g/l NaCl brine) at 110°C. Experiments were conducted on Benth_28 sample. The injection sequence consisted first of injecting oil in the fully brine saturated sample, from the top, to reach Swi. Then brine is injected from the bottom of the sample until Sorw is reached. At this stage, surfactant formulation is injected from the bottom at a rate of 0.005 cc/min, which corresponds to a linear velocity of 1.6 ft/day.

Figure 8 shows snapshots of 2D saturation maps and saturation profiles taken at different time intervals. The two first profiles, at 32 min and 50 min, show respectively the saturation profile at Swi and Sorw. It can be seen that the capillary end effect observed at Swi is reduced after the brine imbibition resulting in a more uniform saturation profile. Once surfactant reaches the sample, we can see the development of an oil banc traduced by a local increase of the oil saturation. The mean saturation during surfactant injection is reported on Figure 9 as a function of the injected pore volume. We can note that the oil production begins at almost 1.5 PV and that the final oil saturation after 3.3 PV is of 5%, which leads to a recovery factor of OOIP of 92% for an additional oil production of 35%. The small increase in the oil saturation that can be observed at the beginning of surfactant injection (about 5%) is attributed to residual oil trapped at the surface of the sample after waterflood and reintroduced in the sample when surfactant is injected.

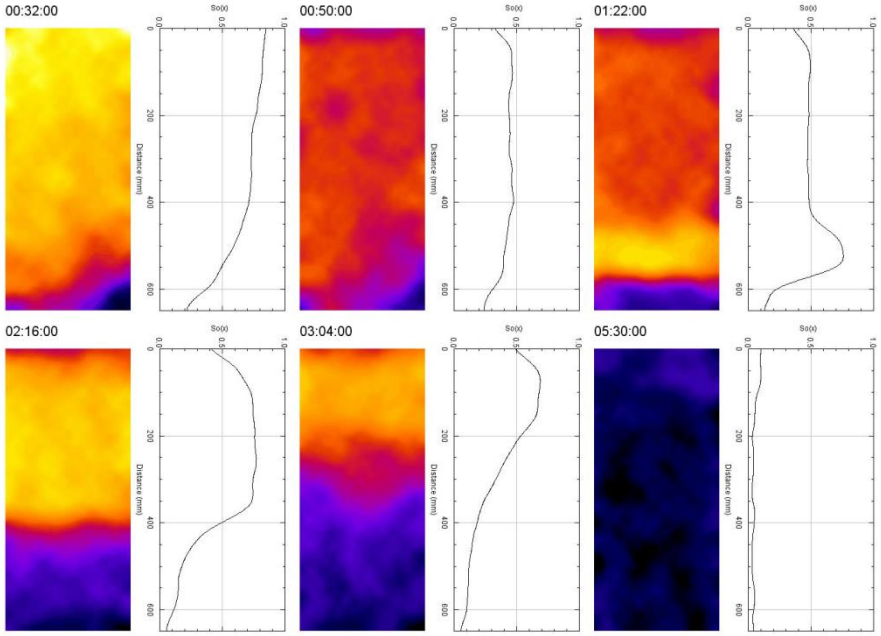

Figure 8 Snapshots of 2D saturation maps and saturation profiles taken at different time intervals for the 110°C experiment (left to right then down left to right). The two first profiles at 32 min and 50 min show respectively saturation profile at Swi and Sorw. Profiles from 1h:22 min to 5h:33 min correspond to surfactant injection at a linear velocity of 1.6 ft/day.

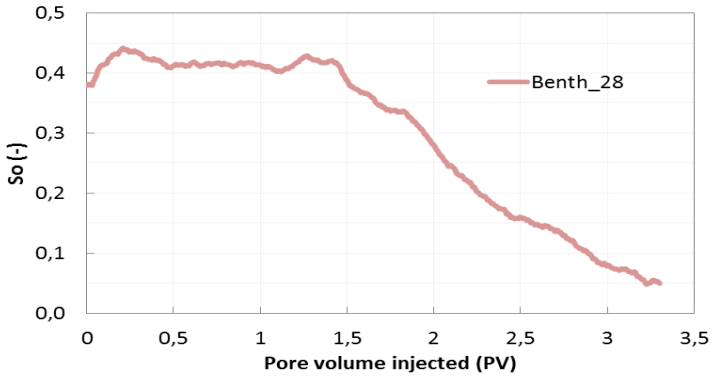

Figure 9 Production curve during the surfactant formulation injection obtained at 110°C. Experiments were conducted on the mini-plug Benth_28.

CONCLUSIONS

In this work, we have presented a new setup and methodologies designed to speed up coreflood experiments by an order of magnitude. The setup (CAL-X) was designed to run experiments on small sample size of 10mm diameter and 20mm length. To validate the setup, we have run a series of experiments on water-wet sandstone samples to determine capillary desaturation curves, steady-state relative permeabilities and recovery factors. Results were satisfactorily compared to standard size core experiments. Integrating this setup in a chemical EOR validation

workflow will not only shorten experimental durations and give quick insights, but also enable exploring a greater parameter space for minimizing uncertainties in the model calibration. Complementary studies are ongoing to extend the workflow to heterogeneous rock type and altered wettability cases.

REFERENCES

[1] Bazin B; Morvan M; Douarche F. and Tabary R. “An Integrated Workflow for Chemical EOR Pilot Design”. SPE IOR Symposium, Tulsa, Oklahoma, USA (2010).
[2] Newsam J. M. “High Throughput Experimentation (HTE) Directed to the Discovery, Characterization and Evaluation of Materials”. Oil Gas Sci. Technol (2015); 70:437.
[3] Selekman J. A; Qiu J; Tran K; Stevens J; Rosso V; Simmons E. and Xiao Y. et al. “High-Throughput Automation in Chemical Process Development”. Annual Review of Chemical and Biomolecular Engineering (2017); 8.
[4] Keelan D. K. "Automated core measurement system for enhanced core data at overburden conditions" Rocky Mountain Regional Meeting of the Society of Petroleum Engineers, Billings, Montana. (1986) SPE-15185.
[5] Maloney D. “X-ray imaging technique simplifies and improves reservoir-condition unsteady-state relative permeability measurements”. Petrophysics (2003); 44.
[6] Griffiths D, Gagea B, Couves J, Spearing M, Webb K. “The Advantages of the Application of Automated Work Flows to Coreflood Testing: Introducing the Next Generation of BP's Advanced EOR Testing Capability” International Petroleum Exhibition and Conference, Abu Dhabi, UAE (2015).
[7] Berg S; Ott H; Klapp S. A; Schwing A; Neiteler R; Brussee N. and Makurat A. et al. “Real-time 3D imaging of Haines jumps in porous media flow”. Proceedings of the National Academy of Sciences of the United States of America (2013); 110:3755–9.
[8] Youssef S; Deschamps H; Dautriat J; Rosenberg E; Oughanem R; Maire E. and Mokso R; "4D imaging of fluid flow dynamics in natural porous media by ultra-fast X-ray microtomography", Int. Sym. of the Society of Core Analysts Napa Valley, California; (2013).
[9] Youssef S; Bauer D; Bekri S; Rosenberg E. and Vizika O; "Towards a better understanding of Multiphase flow in porous media: 3D In-Situ fluid distribution imaging at the pore scale", Int. Sym. of the Society of Core Analysts, Noordwijk aan Zee, The Netherlands; (2009).
[10] Oughanem R; Youssef S; Bauer D; Peysson Y; Maire E. and Vizika O. “A Multi-Scale Investigation of Pore Structure Impact on the Mobilization of Trapped Oil by Surfactant Injection”. Transport in Porous Media (2015); 109:673–92.
[11] Douarche F; Da Veiga S; Feraille M; Enchéry G; Touzani S. and Barsalou R. “Sensitivity analysis and optimization of surfactant-polymer flooding under uncertainties”. Oil Gas Sci. Technol. – Rev. IFP Energies nouvelles (2014); 63.
[12] Oren P.-E; Bakke S. and Arntzen O. J. “Extending predictive capabilities to network models”. SPE journal (1998); 3:324–36.
[13] Oughanem R; Youssef S; Peysson Y; Bazin B; Maire E. and Vizika O. “Pore-scale to core-scale study of capillary desaturation curves using multi-scale 3D imaging”. Int. Sym. of the Society of Core Analysts (2013).